

# A generalized Gross-Pitaevskii model for intersubband polariton lasing

Jacopo Nespolo<sup>1,\*</sup> and Iacopo Carusotto<sup>1,†</sup>

<sup>1</sup>INO-CNR BEC Center and Dipartimento di Fisica, Università di Trento, I-38123 Povo, Italy

(Dated: March 26, 2019)

We develop a generalized Gross-Pitaevskii approach to the driven-dissipative dynamics of intersubband polaritons in patterned planar microcavities where the cavity mode is strongly coupled to an intersubband transition in doped quantum wells. Substantial differences with respect to the case of interband excitonic polaritons are highlighted, in particular the non-Markovian features of the radiative decay. The accuracy of the method is validated on the linear reflection properties of the cavity, that quantitatively reproduce experimental observations. The theoretical framework is then applied in the nonlinear regime to study optical parametric oscillation processes for intersubband polaritons. Our findings open interesting perspectives in view of novel coherent laser sources operating in the mid and far infrared.

Planar semiconductor microcavities have emerged as a versatile tool to address fundamental questions in the physics of light-matter interaction, and realize a new generation of optoelectronic devices, with applications that are still largely unexplored [1]. In particular, a rich variety of optical phenomena are observed when a quantum well element is embedded in the cavity layer and an electronic transition is resonantly coupled to the cavity mode. Depending on the structure and the doping level of the quantum well, the transition can be of either *inter-band* [2] or *inter-subband* nature [3]: in the former case, it involves some electrons being promoted from the valence to the conduction band and is typically located in the near-infrared or visible domain. In the latter case, electrons (or holes) are promoted from a filled subband of the conduction (or valence) band to another, initially empty subband. For a strong enough light-matter coupling, photons can undergo several absorption-emission cycles before being lost. In this so-called *strong light-matter coupling* regime, the eigenmodes are superpositions of photonic and matter excitations: depending on the nature of the electronic transition involved, we usually speak of *interband polaritons* or *intersubband polaritons*.

As a few decades of intense theoretical and experimental research have shown, interband (IB) polaritons combine the extremely low mass of cavity photons (orders of magnitude lower than the excitonic one) with sizable interactions stemming from their excitonic component. These remarkable properties have been at the heart of the celebrated observations of Bose-Einstein condensation [4] and superfluidity effects [5, 6] in a polariton gas and are still being widely exploited in a number of exciting directions, as reviewed in [1, 7, 8].

Since with the early observations [9, 10], the research on intersubband (ISB) polaritons has also made impressive steps. In addition to their operation at much longer wavelengths in the mid or far infrared (MIR or FIR, re-

spectively), ISB polaritons display a few other remarkable differences compared to IB ones. Since a large number of electrons are involved in the optical transition, the Rabi splitting can be pushed to extremely high values just by increasing the doping level in the well, in some cases even comparable to the transition frequency in the so-called *ultra-strong* light-matter coupling regime as predicted in [11, 12] and experimentally observed in [13–15]. The strong coupling to the electromagnetic field displayed by ISB transitions is typically associated to much faster decay processes, which have so far limited the Q-factor of the polariton modes well below 100: while this is well enough to clearly observe the polariton mode splitting [9, 10, 14, 16], relatively high pump intensities are needed to clearly observe nonlinear phenomena [17, 18]. In spite of these difficulties, a wide community is actively involved in the study of nonlinear optical phenomena in these systems, from new sources of coherent light in the MIR/FIR domain based on parametric oscillation [19, 20], Bose-Einstein condensation [21], or inter-polariton transitions [22], to the development of optical comb sources [23, 24], to the generation of nonclassical states of light [11, 25].

Except for the above-cited works, the theoretical study of these processes is still lacking a microscopic model of interaction between ISB polaritons and an flexible and easily manageable theory to describe nonlinear processes with ISB polaritons in different configurations and geometries. While the former issue will be the subject of a forthcoming work [26], the goal of the present article is to introduce a generalized Gross-Pitaevskii equation (GGPE) to describe the nonlinear spatio-temporal dynamics of ISB polaritons. Even though our discussion will be focussed on a specific family of patterned cavities currently used in experiments [27, 28], our GGPE approach has a much wider application range to generic laterally patterned planar devices.

Our theory is of course inspired by an analogous description of IB polaritons, but new technical difficulties originate in ISB systems from the much wider range of frequencies covered by the polaritons and the consequent importance of non-Markovian effects in the radiative de-

\* e-mail: jacopo.nespolo@unitn.it

† e-mail: iacopo.carusotto@unitn.it

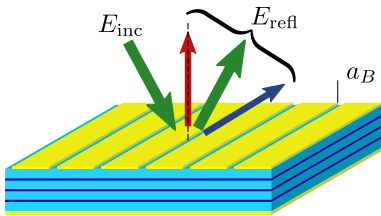


FIG. 1. (Color online) Sketch of the microcavity device under consideration. A series of quantum wells (dark blue) is embedded in a planar microcavity device enclosed by a pair of metallic mirrors (yellow). The top mirror is laterally patterned into a grating to ensure radiative coupling of the cavity modes with the external radiation. The device is operated by shining a pump beam of electric field  $E_{\text{inc}}$  at an angle to its surface. The reflected field  $E_{\text{refl}}$  is dominated by the specular reflection of the pump, but nonlinear phenomena can give rise to other spectral components.

cay. In contrast to IB polaritons whose radiative coupling is typically weakly dependent on frequency and momentum in the region of interest [7], special care is required in the ISB case to correctly enforce the light cone condition on the external propagating modes. This challenge is the main theoretical contribution of this work.

The power of our theory is confirmed by successfully comparing its predictions with experimental reflection spectra obtained in the linear regime [27, 28]. As a first concrete application of the theory, we will take inspiration from related experiments with IB polaritons [7, 29–31] and study the possibility of optical parametric oscillation processes for ISB polaritons. The potential of these processes to realize novel sources of coherent light in the MIR and FIR domains is finally sketched.

The structure of the article is the following. In Sec. I we review the physical system under consideration and we introduce the theoretical model based on the GGPE. The crucial novelty of the approach is summarized in Sec. IB, which deals with the non-Markovian features appearing in the radiative coupling of ISB polaritons with the external radiation. The quantitative accuracy of the method is illustrated in Sec. II, where we present computed reflectivity spectra in striking agreement with experimental observations presented in the recent literature. First applications of the GGPE approach to nonlinear problems are presented in the following Section: results for triply-resonant optical parametric oscillation are presented in Sec. III A, while pump-probe optical amplification is studied in Sec. III B. Conclusions and perspectives are finally summarized in Sec. IV.

## I. THE PHYSICAL SYSTEM AND ITS MODELING

The physical system under consideration is sketched in Fig. 1. It consists of a solid state device featuring a series of two dimensional quantum wells (QW) embedded in a planar semiconductor microcavity. The cavity mode is

enclosed by a pair of plane-parallel metallic mirrors and is able to propagate along the  $xy$  cavity plane. Since we are interested in maximizing the interaction to the ISB transition, we focus our attention on TM-polarized electromagnetic modes with a uniform profile along  $z$  and a wavevector parallel to the cavity plane. This allows to have an electric field fully polarized along the  $z$  direction of the intersubband dipole. In contrast to the case of distributed Bragg reflector microcavities used for IB polaritons, the cavity modes under examination here have a linear, massless dispersion

$$\omega_C(\mathbf{k}) = c|\mathbf{k}|/n \quad (1)$$

with a background refractive index  $n$  of the cavity material on the order of  $n \approx 3$  for typical samples. This means that the photon dispersion in the unpatterned cavity lies below the light cone  $\omega = c|\mathbf{k}|$  and is thus decoupled from external radiative modes.

In order to overcome this limitation, the front mirror is laterally patterned as a Bragg grating along  $x$ . The spatial periodic modulation along the cavity plane induces a Bragg-folding of the dispersion, which enables an effective coupling to the external radiative modes outside the cavity. The period of the grating selects the operation wavelength: in the experiments [16, 27, 28], the operation wavelength is located in the neighborhood of the second Bragg gap which opens around  $\mathbf{k} = 0$ . A typical experiment then consists of sending one (or more) incident beam(s) onto the device and collecting the light that is elastically reflected by the system and/or the new frequency components that are generated by the optical processes taking place inside the cavity. As usual in planar microcavities, the in-plane wavevector of the polaritons directly reflects into the angle made by the external radiation to the normal [7].

Within the wavevector range of optical interest, ISB transitions are nondispersive, at a momentum-independent frequency  $\omega_X = \omega_{\text{ISB}}$ . Since they involve the motion of charged carriers, they are affected by Coulomb interactions between carriers. This is expected to result in strong two-body interactions between intersubband excitations, which then translate into efficient two-body scattering processes between polaritons or, in optical terms, sizable  $\chi^{(3)}$  nonlinear optical susceptibilities.

### A. Conservative light-matter coupling: intersubband polaritons

The dynamics of the photonic cavity field  $\psi_C(\mathbf{r})$  and of the ISB excitonic field  $\psi_X(\mathbf{r})$ , and the strong light-matter interactions occurring between the two, can be cast in terms of a pair of coherently coupled generalized Gross-Pitaevskii equations (GGPE) [7], extending to the nonequilibrium polariton case the formalism used in the context of Bose-Einstein condensates of ultracold atoms,

$$i\partial_t\psi_C(\mathbf{r}) = \left[ \omega_C(-i\nabla) - \frac{i}{2}\gamma_{\text{nr}} \right] \psi_C(\mathbf{r}) + V(x)\psi_C(\mathbf{r}) + \Omega_R\psi_X(\mathbf{r}) - \Gamma_{\text{rad}}(\mathbf{r}, t) + \Pi(\mathbf{r}, t), \quad (2)$$

$$i\partial_t\psi_X(\mathbf{r}) = \left[ \omega_X - \frac{i}{2}\gamma_h \right] \psi_X(\mathbf{r}) + \frac{g}{2}|\psi_X(x)|^2\psi_X(\mathbf{r}) + \Omega_R\psi_C(\mathbf{r}). \quad (3)$$

The nonradiative losses of the cavity mode and the homogeneous losses of the ISB excitations are represented by the coefficients  $\gamma_{\text{nr}}$  and  $\gamma_h$ , respectively, and they are assumed to be local and homogeneous in space. The strength of the coherent light-matter coupling is quantified by the Rabi frequency  $\Omega_R$ . To reduce the technicalities, we focus our attention here on the case of a strong but not ultra-strong coupling, in which  $\omega_{X,C} \gg \Omega_R \gg \gamma$ .

Since a complete theory of interactions between inter-subband excitations is still in the course of being developed [26], these are modeled here in the simplest way as spatially local binary interactions of strength  $g$ . Since the value of this quantity is still unknown, throughout this work we will express interaction energies in terms of the experimentally observable blue-shift  $g|\psi_X|^2$ .

The effect of the Bragg grating is the most subtle one and is responsible for the main differences compared to the case of IB polaritons. On one hand, it introduces into the GGPE an external potential  $V(x)$  term acting on the photonic field, diagonal in coordinate space and periodic with period  $a_B$ . On the other hand, new Bragg-scattering-mediated radiative channels exist, through which light can be injected (extracted) into (from) the cavity.

### B. Effect of pump and losses

The last two terms in Eq. 2 account for the radiative losses ( $\Gamma_{\text{rad}}$ ) and the external pumping of the cavity field ( $\Pi$ ). In the case of IB polaritons all  $\mathbf{k}$ -modes involved in the dynamics are radiative and can be described [7] within a Markovian theory in terms of a (almost) frequency- and momentum-independent radiative loss rate  $\gamma_C$ . Here, the Bragg-folded cavity dispersion crosses the light cone, which requires the frequency-dependence to be explicitly included and gives rise to non-Markovian features in the decay process. An efficient modeling of this physics in the GGPE framework is the subject of this section.

The incident field  $E_{\text{inc}}(\mathbf{k}, \omega)$  only involves propagating radiative modes satisfying the light-cone condition  $\omega \geq c|\mathbf{k}|$ . Even though no direct resonant coupling to the optical modes of an unpatterned planar cavity can occur, Bragg scattering processes on the grating are effective in relaxing this condition, as sketched in Fig. 2. This can be

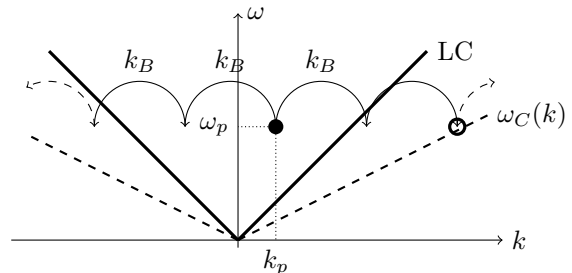


FIG. 2. Sketch of the Bragg scattering-mediated coupling of cavity modes to external radiation. An incident photon (full circle) of in-plane momentum  $k_p$  and frequency  $\omega_p$  must lie within the radiative region above the lightcone (LC) indicated by the full line. The incident light wavevector changes by multiples of the Bragg wave number  $k_B$  as a consequence of the scattering on the grating, thus allowing to resonantly couple to the cavity mode (open circle).

formally captured by the relation

$$\tilde{\Pi}(\mathbf{k}, \omega) = \int \mathcal{T}(\mathbf{k}, \mathbf{k}') \tilde{E}_{\text{inc}}(\mathbf{k}', \omega) d\mathbf{k}', \quad (4)$$

between the Fourier components of the in-cavity and radiative fields, where the convolution kernel  $\mathcal{T}(\mathbf{k}, \mathbf{k}')$  acts as a generalised transmission coefficient. The conjugate of the same transmission coefficient appears in the expression

$$\tilde{E}_{\text{refl}}(\mathbf{k}', \omega) = \tilde{E}_{\text{inc}}(\mathbf{k}', \omega) - i\mathcal{T}^*(\mathbf{k}, \mathbf{k}') \tilde{\psi}_C(\mathbf{k}, \omega). \quad (5)$$

for the radiation emerging from the cavity – also this latter being of course localized in the radiative region  $\omega \geq c|\mathbf{k}|$ .

While the form of these equations is fixed by the general structure of the problem, the detailed form of  $\mathcal{T}(\mathbf{k}, \mathbf{k}')$  depends on the microscopic details of the sample. Given the discrete translational symmetry of the grating,  $\mathcal{T}(\mathbf{k}, \mathbf{k}')$  will consist of a series of  $\delta$ -peaks at  $k_y = 0$  and  $k_x = mk_B$  (with integer  $m$ ), i.e. integer multiples of the Bragg wavevector  $k_B = 2\pi/a_B$ . One can also anticipate that the amplitude of the different  $\delta$ -peaks is a decreasing function of  $|\mathbf{k} - \mathbf{k}'|$  and roughly proportional to the Fourier transform of the potential  $V(x)$  experienced by the cavity mode in Eq. 2, i.e.,

$$\mathcal{T}(\mathbf{k}, \mathbf{k}') \propto \tilde{V}(|\mathbf{k} - \mathbf{k}'|), \quad (6)$$

with the proportionality factor set phenomenologically to reproduce the physical linewidth of a reference cavity

band. In our calculations, we do this with respect to the third photonic band (cf. Fig. 3).

More care is needed for the radiative loss term  $\Gamma_{\text{rad}}$ . This is once again due to the strong frequency dependence of the spectral density of the radiative modes, that are spectrally localized above the light-cone  $\omega \geq c|\mathbf{k}|$ . Below it, the spectral density of radiative modes is rigorously zero. This introduces non-Markovian features in the dissipative dynamics [32].

If both the incident and the cavity fields are monochromatic at frequency  $\omega$ , it is enough to evaluate the decay at the given frequency  $\omega$ , so that radiative losses can be directly included into the GGPE as temporally local  $\mathbf{k}$ -space terms

$$\tilde{\Gamma}_{\text{rad}}(\mathbf{k}, t) = -\frac{i}{2} \int d\mathbf{k}'' \Gamma_{\omega}(\mathbf{k}, \mathbf{k}'') \psi_C(\mathbf{k}'', t) d\mathbf{k}'', \quad (7)$$

where the integral in the kernel

$$\Gamma_{\omega}(\mathbf{k}, \mathbf{k}'') = \int_{|\mathbf{k}'| \leq \omega/c} d\mathbf{k}' \mathcal{T}^*(\mathbf{k}'', \mathbf{k}') \mathcal{T}(\mathbf{k}, \mathbf{k}') \quad (8)$$

runs over those intermediate radiative modes  $\mathbf{k}'$  lying above the light-cone. The small shift of the cavity modes due to the coupling to the radiative modes outside the cavity has been neglected. In its simplicity, this exactly solvable single-frequency case encompasses polariton superfluidity experiments [5] and quantum hydrodynamic soliton nucleation [6]: whereas this physics has been so far studied only in the exciton-polariton case, our theory provides an efficient tool to investigate it in the new case of ISB polaritons.

For a general dynamics, the frequency-dependence of the radiative decay leads to a temporally non-local response,

$$\tilde{\Gamma}_{\text{rad}}(\mathbf{k}, t) = -\frac{i}{2} \int d\mathbf{k}'' \int_0^{\infty} d\tau \bar{\Gamma}(\mathbf{k}, \mathbf{k}''; \tau) \psi_C(\mathbf{k}'', t - \tau), \quad (9)$$

where the delay kernel  $\bar{\Gamma}(\mathbf{k}, \mathbf{k}''; \tau)$  is the inverse Fourier transform of  $\Gamma_{\omega}(\mathbf{k}, \mathbf{k}'')$  with respect to  $\omega$ , and accounts for both dissipative and reactive effects of the coupling to the radiative modes [33]. Since the temporal non-locality of  $\bar{\Gamma}$  introduces technical difficulties in the solution of the GGPE Eqs. 2-3, for practical problems it is useful to devise approximate treatments that provide accurate results while preserving temporal locality.

Unless one is dealing with features lying near to the edge of the light cone, a natural strategy to this purpose is the approximate  $\Gamma_{\omega}(\mathbf{k}, \mathbf{k}'')$  with its value at the bare mode frequencies. In our case, it is convenient to choose  $\omega = c(|\mathbf{k}| + |\mathbf{k}'|)/2$ , which has the advantage of being symmetric under exchange of  $\mathbf{k}$  and  $\mathbf{k}'$  and to recover the common value when the frequencies of the two modes coincide and the damping term is most effective. In the next sections we will make use of this prescription and we will see that it provides accurate and predictive results.

Our numerical implementation uses the so-called split-step method to include the potential and the kinetic energy in the GGPE as diagonal terms in either real- or momentum-space, and to use a standard Fast Fourier transform method to quickly switch between them. The pump and radiative damping terms, which are not diagonal in neither real- nor momentum-space, are implemented by first order discretisation of time at the end of each split-step evolution interval. To reduce the numerical load, the simulations are carried out in the rotating frame in which the carrier pump mode is stationary.

The convergence of the results was assessed by simulating the same system on progressively finer meshes. As a rule of thumb, it was found that results are converged when  $a_B/\Delta x \gtrsim 8$ .

In the definition of the matrix  $\mathcal{T}(\mathbf{k}, \mathbf{k}')$  there are two implementation subtleties that the reader should be aware of. First, the spectrum of the Bragg potential,  $\tilde{V}(\mathbf{k})$ , must decay sufficiently fast to zero for large wavenumbers in order for the simulation to converge as the mesh is refined. Depending on the particular Bragg pattern, it may be convenient to smoothen down large wavenumber components of the potential according to an exponential law. Second, the lightcone condition introduces sharp edges, which may give rise to high frequency and high wavenumber artifacts. Once again, the solution is to smoothen the edge of the lightcone according to an exponential law.

In order to simplify the technicalities, we assume that the grating is homogeneous along the  $y$  direction and we focus our attention on light fields at  $k_y = 0$ . Under these assumptions, a one-dimensional version of the GGPEs can be used. If needed, no conceptual difficulty would prevent our results from being straightforwardly extended to two dimensional patterns and arbitrary in-plane wavevectors and incidence angles.

## II. LINEAR OPTICS

For sufficiently weak driving, we can assume that linear response is a satisfactory description. Indeed, without a sufficient build up of the ISB excitonic modes, the contribution  $g|\psi_X|^2$  to the total energy is negligible when compared to the other energy scales at play in Eq. 3.

Reflection measurements are a powerful tool to gain knowledge of the physics taking place inside the micro-cavity. The reflected intensity  $I_{\text{refl}}(\mathbf{k}, \omega) = |\tilde{E}_{\text{refl}}(\mathbf{k}, \omega)|^2$  is a relatively easy measurement in experiments. The in-plane wavenumber can be selected by changing the angle at which one collects (shines) the reflected (incident) radiation, and channeling the radiation through a Fourier transform spectrometer gives access to the spectral distribution.

Referencing the reflected field to the incident one, we



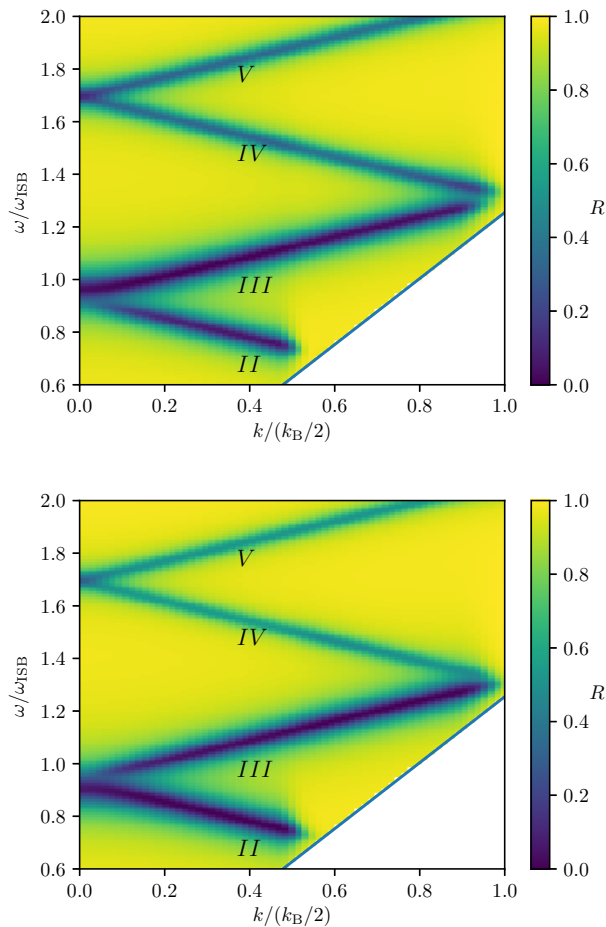


FIG. 3. (Color online) Colorplots of the frequency- and momentum-dependent reflectivity  $R(\mathbf{k}, \omega)$  for empty cavities, i.e.,  $\Omega_R = 0$ . The Bragg grating consists of a square wave potential of period  $a = 4.26 \mu\text{m}$  with filling factor 75% (top panel, comparable to the device used in Ref. [28]) and 25% (bottom panel). The remaining simulation parameters are reported in Appendix A. Roman numerals label the order of each band. The different visibility of the bands is the sole consequence of the different filling factor. The diagonal solid line indicates the light-cone condition: the white region below it in the bottom-right direction is inaccessible to reflection experiments.

recover the usual definition of the reflectivity,

$$R(\mathbf{k}, \omega) = \frac{I_{\text{refl}}(\mathbf{k}, \omega)}{I_{\text{inc}}(\mathbf{k}, \omega)} = \frac{|\tilde{E}_{\text{refl}}(\mathbf{k}, \omega)|^2}{|\tilde{E}_{\text{inc}}(\mathbf{k}, \omega)|^2}, \quad (10)$$

which we are going to use extensively in the following sections. Plots of the reflectivity in different cases are shown in Fig. 4.

A more in depth experimental investigation can benefit from electro-optic sampling techniques, allowing the real time measurement of the actual reflected electric field  $\tilde{E}_{\text{refl}}(\mathbf{k}, t)$  [34–40]. The direct measurement of both amplitude and phase of the reflected radiation allows to

study more subtle optical features such as the temporal shape of wavepackets or the coherence properties of the emission.

### A. Bare cavity

It is instructive to first consider the case of an empty cavity, in which no ISB transition is present or, equivalently, this is decoupled from the cavity field  $\Omega_R = 0$ . Because of the grating, the linear dispersion of the free photon is folded around the first Brillouin zone and gaps open because of Bragg scattering processes.

Examples of reflectivity spectra in the  $(k_x, \omega)$  plane at  $k_y = 0$  for an empty cavity and two different gratings are shown in Fig. 3. In the reflectivity plots, the photonic bands show up as reflectivity minima, or, in other words, as peaks in the resonant absorption of the incident field.

The physical parameters of the calculation were chosen so as to closely match the devices used in current experiments [41], cf. App. A. The grating is included in the GGPE as

$$V(x) = V_0 \begin{cases} 2 - 2\nu & \text{if } 0 \leq x \bmod a_B \leq \nu a_B, \\ -2\nu & \text{if } \nu a_B < x \bmod a_B \leq 1, \end{cases} \quad (11)$$

i.e., a zero-mean square wave of amplitude  $V_0$ , period  $a_B$  and filling factor  $\nu$ . The results in Fig. 3 only differ by the filling factor of the grating, namely,  $\nu = 75\%$  and  $\nu = 25\%$  for top and bottom panels, respectively, the former being representative of the experimental conditions [27, 28]. The visibility of the different bands changes with the details of the Bragg grating. For instance, the second band tends to fade towards  $k = 0$  and the third band is more pronounced at high filling factors, whereas the opposite is true for low filling. In the symmetric case (50% filling, not shown), both bands are approximately equally visible.

This shows that our modelling of the pumping and of the radiative losses in terms of the transmission matrix  $\mathcal{T}(\mathbf{k}, \mathbf{k}')$  as described in Sec. IB is able to capture the nuances and complexities of the grating potential without the need to manually tune any parameter, as it was instead the case in the temporal coupled-mode theory of Ref. [28]. As a result, more complicated gratings can be studied without the need to modify the general structure of the model, which can be readily extended to fully two dimensional geometries, too.

### B. Strong coupling regime

Still in the weak pump limit, we now allow for nonzero values of the Rabi coupling  $\Omega_R$ , so that the system can enter the strong coupling regime. The reflectivity for this case is displayed in Fig. 4. As expected, there is a clear avoided crossing between the non-dispersive ISB transition at  $\omega_{\text{ISB}}$  and the bare cavity photonic dispersion,

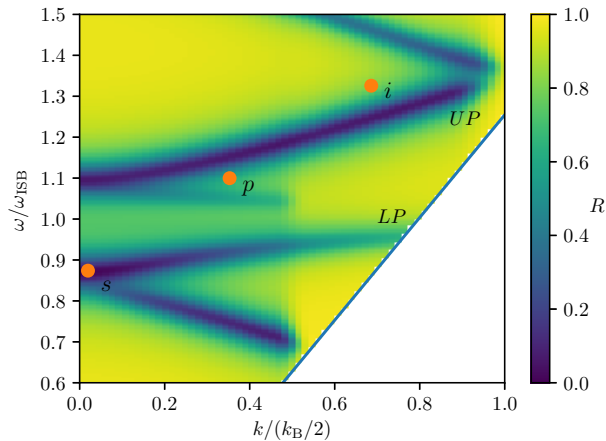


FIG. 4. (Color online) Reflectivity  $R(\mathbf{k}, \omega)$  of cavity modes strongly coupled to an intersubband transition. The simulation parameters are reported in Appendix A. The dots indicate the pump, signal, and idler modes of the OPO discussed in Sec. III A.

with the appearance of the typical upper and lower polariton branches separated by a gap of the order of  $2\Omega_R$ . In between the two main polariton bands indicated as LP and UP in Fig. 4, weak additional bands of dominant ISB character appear in the energy region around  $\omega_{\text{ISB}}$ . Their physical origin is due to the Bragg folding of the main polariton branches.

The accuracy of this approach is apparent when this plot for the reflectivity is compared to experimental measurements reported, e.g., in Ref. [27, 28]. In contrast with the phenomenological temporal coupled-mode theory used in the works cited, we provide a more microscopic treatment, which can be straightforwardly extended to more complex geometries as well as to the far richer nonlinear physics in the presence of interactions between polaritons. This topic is the subject of the next Section.

### III. NONLINEAR OPTICS

As the intensity of the incident beam is increased, nonlinear phenomena start to play a crucial role in the dynamics. Nonlinearities, arising from polariton-polariton scattering—or from other channels not discussed in the present paper—will in general shift the energy position of the bands in a nontrivial way. The resonance condition between the incident pump and the energy shifted bands, and the in-cavity mode mixing and frequency conversion processes act together in a complex way, giving origin to a variety of nonlinear effects. A review of the most significant nonlinear effects in the context of IB exciton polaritons is given in Ref. [7].

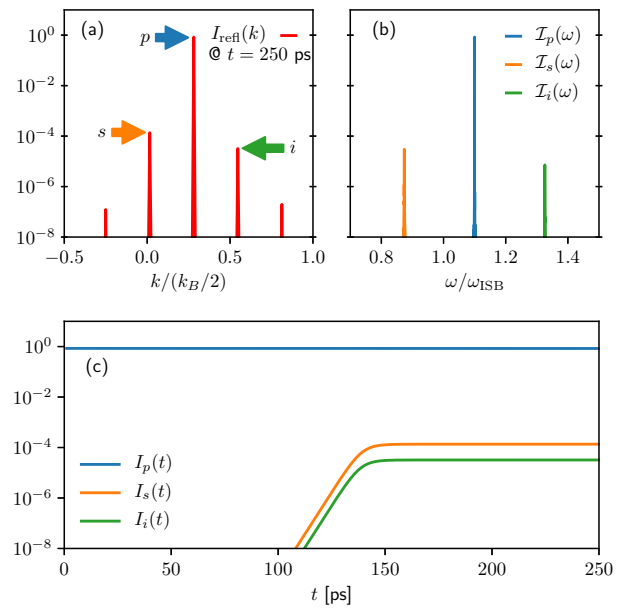


FIG. 5. (Colour online) Optical parametric oscillation under continuous-wave pumping at  $k_p/(k_B/2) \approx 0.28$ ,  $\omega_p/\omega_{\text{ISB}} = 1.1$  and the simulation parameters of App. A. The positions of the pump, signal and idler are marked by dots in Fig. 4. The pump intensity and nonlinear coupling are tuned such that  $g/|\psi_X|^2 = 23.1$  meV. All intensities are normalised to the intensity of the pump mode. (a) Steady state (in practice computed after 250 ps of evolution)  $k$ -space momentum distribution of the emitted radiation. Besides the signal and idler peaks, one sees further replicas due to higher order diffraction from the grating. (b) Momentum-selected (i.e., angle-selected) emitted radiation spectrum in the frequency domain,  $\mathcal{I}_{\{p,s,i\}}(\omega) = I(k_{\{p,s,i\}}, \omega)$  (c) Intensities of pump, signal and idler emission in real time,  $I_{\{p,s,i\}}(t) \equiv I_{\text{refl}}(k_{\{p,s,i\}}, t)$

#### A. Optical parametric oscillation

If the pump parameters are carefully tuned to resonantly excite suitable points ( $\mathbf{k}_p, \omega_p$ ) on the polaritonic bands, the system may enter the so-called optical parametric oscillation (OPO) regime. In this regime, two pump polaritons are resonantly scattered to another pair of states, commonly known as *signal* and *idler* (hereafter noted with subscripts  $s$  and  $i$ , respectively). The peculiar shape of the polaritonic band structure may in fact allow for the scattering process to be triply-resonant, with pump, signal and idler all lying on the dynamically shifted polaritonic bands. In this case, energy and momentum are conserved during the elementary parametric scattering process underlying OPO,

$$\mathbf{k}_i + \mathbf{k}_s = 2\mathbf{k}_p, \quad \omega_i + \omega_s = 2\omega_p. \quad (12)$$

As typical of bosons, a nonvanishing population in the final states further stimulates the scattering process. The signal and idler states may then become macroscopically

occupied if the pump is strong enough to overcome losses, and may emit coherent radiation, normally with a narrow distribution in both wavenumber (i.e., angle) and frequency [7]. The main result of this section is that the ISB polariton system can support polariton OPO operation.

While excitonic polaritons are studied in the visible or near-IR ranges, and are bound to the vicinity of the electronic band gap of the material, ISB systems allow for OPO operation in the novel spectral windows of MIR and THz frequencies, with a very wide tunability range: the Bragg frequency  $ck_B$  of the cavity is simply determined by the grating period, while  $\omega_{\text{ISB}}$  is controlled by the QW thickness. This flexibility will be of paramount technological importance when one is to design OPO sources operating at a given desired frequency. To facilitate the application of our results to different frequency ranges, our results will be plotted in units of  $\omega_{\text{ISB}}$ .

Figure 5(a, b) show the emission spectra as predicted via a numerical simulation of the coupled GGPEs (2-3) using realistic physical parameters. The drive is a monochromatic pump at energy  $\omega/\omega_{\text{ISB}} = 1.1$  and  $23.3^\circ$  angle of incidence, i.e., wavenumber  $k_p \approx 0.28(k_B/2)$ . An extremely weak random noise was added to the simulation to seed the scattering process. The signal and idler are emitted at  $k_s \approx 0.02$  and  $k_i \approx 0.55$  in units of  $k_B/2$ , at frequencies  $\omega_s \approx 0.87\omega_{\text{ISB}}$  and  $\omega_i \approx 1.33\omega_{\text{ISB}}$ , respectively. The triplet of pump, signal and idler obtained from the simulation is also marked with dots in the linear regime band diagram of Fig. 4. Their slightly shifted position out of resonance from the band is due to the significant blue shift of the upper polaritonic band due to the same polariton-polariton interactions that are responsible for the parametric scattering process.

As shown in Fig. 5(c), the emission from the signal and idler states grows in intensity over approximately 150 ps, after which the system reaches a steady OPO state. However, this time scale wildly varies with the fine details of the system. Due to the stimulated character of the scattering process, the time required to reach the steady state is sensitive to the amount of initial noise that seeds the scattering process, and the actual nature and strength of the nonlinear coupling. Because of these limitations, we cannot assess the OPO threshold in terms of a physical pump intensity. Nonetheless, this can be estimated in terms of the nonlinear frequency shift  $g|\psi_X|^2$ , and is of the order of a few decay rates. For the realistic parameters of [28], this would amount to around 15 meV. A specific study of the polariton interaction constant  $g$  for different QW shapes and different levels of electronic doping is subject of on-going work [26]: its main result will be a quantitative prediction for the value of the incident pump intensity at the OPO threshold.

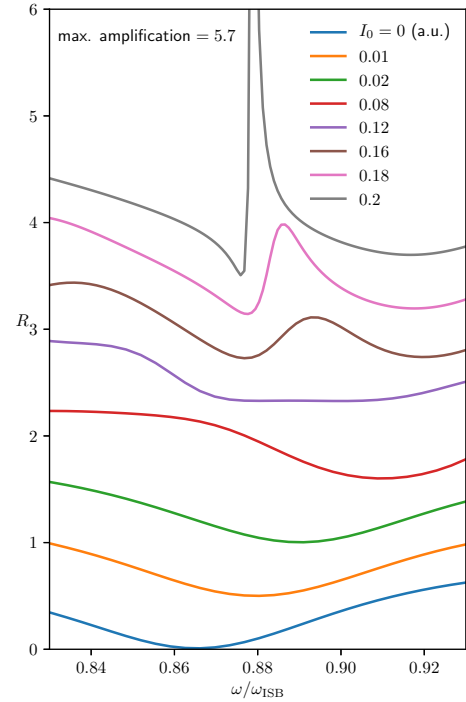


FIG. 6. Emission spectra with continuous wave pump ( $\omega/\omega_{\text{ISB}} = 1.065$ ,  $k/(k_B/2) \approx 0.28$ ) and 150 fs long Gaussian probe pulses ( $\omega/\omega_{\text{ISB}} = 0.89$ ,  $k = 0$ ) of growing intensity  $I_0$ , always below the OPO threshold located at  $I_0^{\text{thr}} \approx 0.22$  in these units. The probe intensity is taken very weak at  $10^{-10}$ . For clarity, each curve is offset by 0.5 from the previous one.

## B. Optical amplification in pump-probe configuration

Even below the threshold for a fully developed OPO, polariton-polariton scattering is able to transfer polaritons from the pump state to the signal and idler states. This phenomenon can be used to achieve optical amplification in a standard pump-probe configuration. An intense beam, ideally spectrally narrow, resonantly pumps the system, while a weaker probe beam, often spectrally broad, is shone so as to populate the final signal state, thus stimulating the scattering process. The onset of optical amplification is then witnessed by an intense narrow peak within the otherwise broad probe spectrum.

### 1. Continuous wave pump

We first consider the ideal case of a continuous wave pump below the threshold intensity of OPO. Figure 6 shows the  $k = 0$  emission spectra for increasing pump intensity. A monochromatic pump ( $\omega/\omega_{\text{ISB}} = 1.065$ ,  $k/(k_B/2) \approx 0.28$ ) is paired with a 150 fs Gaussian probe pulse at  $k = 0$ , centered at  $\omega/\omega_{\text{ISB}} = 0.89$ . For this choice of parameters, the probe is approximately resonant with

the lower polariton branch, yet with a much broader linewidth. Its intensity is extremely weak, to guarantee that the dynamics is deeply in the linear regime with respect to the probe amplitude.

As the pump intensity  $I_0$  is ramped up, the first feature found in the numerics is a blue shift of the lower polariton minimum from its linear regime position (shown by the  $I_0 = 0$  curve in the figure). Most remarkably, an experimental measurement of this lineshift as a function of the pump intensity would provide a useful estimate of the actual strength of the nonlinear coupling  $g$  and of the OPO threshold intensity. Simultaneous recording of all polariton branches would shine light on the precise mechanism underlying polariton-polariton interactions [42]. Further increasing the pump intensity, the emission spectra develop a peak that, sufficiently close to the threshold pump amplitude, becomes a sharp optical amplification signal.

We stress that an increase in the probe reflectivity at a given  $(\mathbf{k}, \omega)$  is not a firm evidence of a parametric scattering process. Such an increase can in fact originate from other effects, e.g., an increased polariton linewidth. Instead, the observation of a line narrowing effect and—especially—the direct detection of the third idler beam in addition to the pump and probe beams (typically at larger angles and frequencies) would be strong evidences that optical amplification is indeed taking place in the system.

## 2. Pulsed pump

Since no experimental measurement of the polariton-polariton interaction constant is available yet, we can not exclude that reaching the OPO threshold might require such high intensities that the only option could be the use of pulsed pump sources, all the way down to picosecond pulses or shorter. For such short pulses, peak intensities up to  $\text{GW}/\text{cm}^2$  are in fact within reach of state-of-the-art sources.

In Fig. 7(a) we show the spectra obtained by driving the system with Gaussian pump pulses of increasing duration. The carrier frequency of the pump is the same of the previous subsection, as are the parameters of the probe. By stretching the pump duration, the system has time to build up population in the pump mode. When the pump is too short, parametric scattering processes do not have the time to efficiently amplify the probe. On the other hand, when the pump pulse is longer than approximately 3 ps, the scattering of polaritons from the pump to signal and idler states is strong enough to give an observable amplification of the probe.

This result should be seen as a proof of principle; given the very complex and sometimes even chaotic dynamics of OPOs, the time duration of the pump pulse required to reach actual amplification may depend on the fine details of the sample under consideration, as well as on the details of the pump-probe set-up and timing. As a general feature, we have observed a high sensitivity to the time

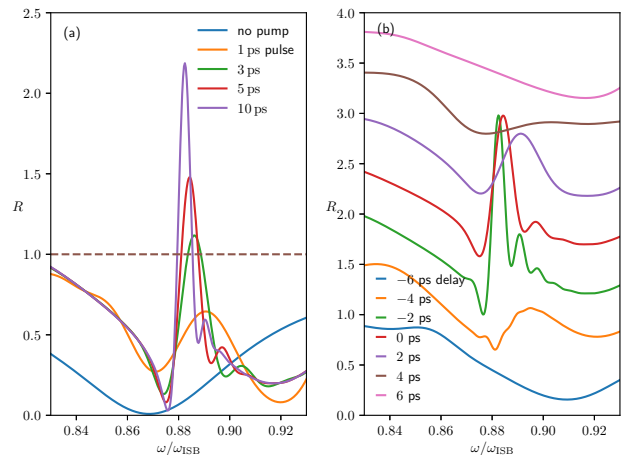


FIG. 7. Emission spectrum with pulsed pump of peak intensity  $I_0 = 0.2$  in the units used in Fig. 5,  $\omega/\omega_{\text{ISB}} = 1.065$ ,  $2k/k_B \approx 0.28$  and 150 fs Gaussian pulse probe ( $\omega/\omega_{\text{ISB}} = 0.89$ ,  $k = 0$ ,  $I_0 = 10^{-5}$ ). (a) The pump is a Gaussian packet of increasing duration. The pump and probe pulses are synchronised so that they reach their maximum intensity at the same time. For pump pulses longer than approximately 3 ps, amplification is observed. (b) Effect of time delay between the probe and the pump pulse using under 5 ps pulsed pump. Curves are offset by 0.5 for clarity.

delay between the arrival of the two pulses, as shown in Fig. 7(b). It appears that a slightly anticipation of the probe pulse with respect to the arrival of the pump, i.e., a negative delay, may result in higher amplification. This can be intuitively understood as a pre-seeding of the final signal state that has then time to develop during the whole time that the intensity of the pump is at its peak.

## IV. CONCLUSIONS

In this work we presented a new theoretical approach to study the linear and nonlinear dynamics of ISB polaritons resulting from the strong coupling between a planar cavity mode and an intersubband electronic transition in doped quantum wells. A special attention is paid to the non-Markovian driven-dissipative features occurring in the radiative coupling of the cavity polariton modes to the external radiation ones via Bragg scattering processes, which constitute the main difference from the well-known case of IB polaritons. The quantitative power of our approach is validated on the linear reflection spectra, that successfully reproduce the ones observed in recent experiments [27, 28]. As a first example of concrete application, we studied optical parametric oscillation processes between intersubband polaritons and we outlined their perspectives in view of a new concept of coherent intersubband polariton laser sources [21] operating in the MIR and FIR spectral domains.



While experimental studies in this direction are actively in progress, new theoretical steps include a quantitative study of the microscopic interaction between polaritons [26] and an extension of our theory to the ultrastrong coupling regime [11, 43], in which the non-rotating wave terms introduce substantial further complications in the treatment of the radiative decay channels.

We acknowledge financial support from the European Union FET-Open grant MIR-BOSE (737017) and from the Provincia Autonoma di Trento. We are grateful to C. Ciuti, R. Colombelli, M. Knorr, C. Lange, S. De Liberato and H.A.M. Leymann for continuous stimulating discussions.

## Appendix A: System parameters

Unless otherwise stated, the system parameters used in the simulations are the following:  $\omega_{\text{ISB}} = 116$  meV,  $n = 3.3$ ,  $\omega_0 = 20$  meV,  $\gamma_{\text{nr}} = 5.4$  meV,  $\gamma_{\text{r}} = 4.5$  meV,  $\gamma_{\text{h}} = 6.0$  meV,  $V_0 = 10$  meV,  $a_B = 4.26$   $\mu\text{m}$ , filling factor  $\nu = 75\%$  and  $\Omega_R = 13$  meV. This choice of parameters is informed by the physical device used in the experiments of Ref. [28].

- 
- [1] A. V. Kavokin, J. J. Baumberg, G. Malpuech, and F. P. Laussy, *Microcavities* (OUP Oxford, 2017).
  - [2] P. Yu and M. Cardona, *Fundamentals of Semiconductors: Physics and Materials Properties* (Springer Berlin Heidelberg, 2005).
  - [3] H. C. Liu and F. Capasso, *Intersubband Transitions in Quantum Wells: Physics and Device Applications* (Academic Press, 1999).
  - [4] J. Kasprzak, M. Richard, S. Kundermann, A. Baas, P. Jeambrun, J. M. J. Keeling, F. M. Marchetti, M. H. Szymaska, R. Andr, J. L. Staehli, V. Savona, P. B. Littlewood, B. Deveaud, and Le Si Dang, “BoseEinstein condensation of exciton polaritons,” *Nature* **443**, 409 (2006).
  - [5] A. Amo, J. Lefrère, S. Pigeon, C. Adrados, C. Ciuti, I. Carusotto, R. Houdré, E. Giacobino, and A. Bramati, “Superfluidity of polaritons in semiconductor microcavities,” *Nature Physics* **5**, 805 (2009).
  - [6] A. Amo, S. Pigeon, D. Sanvitto, V. G. Sala, R. Hivet, I. Carusotto, F. Pisanello, G. Lemnager, R. Houdr, E. Giacobino, C. Ciuti, and A. Bramati, “Polariton superfluids reveal quantum hydrodynamic solitons,” *Science* **332**, 1167–1170 (2011).
  - [7] I. Carusotto and C. Ciuti, “Quantum fluids of light,” *Rev. Mod. Phys.* **85**, 299 (2013).
  - [8] T. Ozawa, H. M. Price, A. Amo, N. Goldman, M. Hafezi, L. Lu, M. Rechtsman, D. Schuster, J. Simon, O. Zilberberg, and I. Carusotto, “Topological photonics,” (2018), arXiv:1802.04173.
  - [9] D. Dini, R. Köhler, A. Tredicucci, G. Biasiol, and L. Sorba, “Microcavity polariton splitting of intersubband transitions,” *Phys. Rev. Lett.* **90**, 116401 (2003).
  - [10] E. Dupont, H. C. Liu, A. J. SpringThorpe, W. Lai, and M. Extavour, “Vacuum-field Rabi splitting in quantum-well infrared photodetectors,” *Phys. Rev. B* **68**, 245320 (2003).
  - [11] C. Ciuti, G. Bastard, and I. Carusotto, “Quantum vacuum properties of the intersubband cavity polariton field,” *Physical Review B* **72**, 115303 (2005).
  - [12] Y. Todorov and C. Sirtori, “Intersubband polaritons in the electrical dipole gauge,” *Phys. Rev. B* **85**, 045304 (2012).
  - [13] A. A. Anappara, S. De Liberato, A. Tredicucci, C. Ciuti, G. Biasiol, L. Sorba, and F. Beltram, “Signatures of the ultrastrong light-matter coupling regime,” *Phys. Rev. B* **79**, 201303 (2009).
  - [14] Y. Todorov, A. M. Andrews, R. Colombelli, S. De Liberato, C. Ciuti, P. Klang, G. Strasser, and C. Sirtori, “Ultrastrong light-matter coupling regime with polariton dots,” *Phys. Rev. Lett.* **105**, 196402 (2010).
  - [15] M. Geiser, F. Castellano, G. Scalari, M. Beck, L. Nevou, and C. Sirtori, “Ultrastrong coupling regime and plasmon polaritons in parabolic semiconductor quantum wells,” *Phys. Rev. Lett.* **108**, 106402 (2012).
  - [16] Y. Todorov, A. M. Andrews, I. Sagnes, R. Colombelli, P. Klang, G. Strasser, and C. Sirtori, “Strong light-matter coupling in subwavelength metal-dielectric microcavities at terahertz frequencies,” *Phys. Rev. Lett.* **102**, 186402 (2009).
  - [17] S. Zanotto, R. Degl’Innocenti, J.-H. Xu, L. Sorba, A. Tredicucci, and G. Biasiol, “Ultrafast optical bleaching of intersubband cavity polaritons,” *Phys. Rev. B* **86**, 201302 (2012).
  - [18] S. Zanotto, F. Bianco, L. Sorba, G. Biasiol, and A. Tredicucci, “Saturation and bistability of defect-mode intersubband polaritons,” *Phys. Rev. B* **91**, 085308 (2015).
  - [19] S. De Liberato and C. Ciuti, “Stimulated scattering and lasing of intersubband cavity polaritons,” *Phys. Rev. Lett.* **102**, 136403 (2009).
  - [20] L. Nguyen-thê, S. De Liberato, M. Bamba, and C. Ciuti, “Effective polariton-polariton interactions of cavity-embedded two-dimensional electron gases,” *Phys. Rev. B* **87**, 235322 (2013).
  - [21] R. Colombelli and J.-M. Manceau, “Perspectives for intersubband polariton lasers,” *Phys. Rev. X* **5**, 011031 (2015).
  - [22] S. De Liberato, C. Ciuti, and C. C. Phillips, “Terahertz lasing from intersubband polariton-polariton scattering in asymmetric quantum wells,” *Phys. Rev. B* **87**, 241304 (2013).
  - [23] A. Hugi, G. Villares, S. Blaser, H. C. Liu, and J. Faist, “Mid-infrared frequency comb based on a quantum cascade laser,” *Nature* **492**, 229 (2012).
  - [24] M. S. Vitiello, G. Scalari, B. Williams, and P. De Natale, “Quantum cascade lasers: 20 years of challenges,” *Opt. Express* **23**, 5167–5182 (2015).
  - [25] G. Gnter, A. A. Anappara, J. Hees, A. Sell, G. Biasiol, L. Sorba, S. De Liberato, C. Ciuti, A. Tredicucci, A. Leitenstorfer, and R. Huber, “Sub-cycle switch-on of ultra-

- strong light-matter interaction,” *Nature* **458**, 178 (2009).
- [26] H. A. M. Leymann and I. Carusotto, “Nonlinear response of intersubband transitions in semiconductor quantum wells,” In preparation (2019).
- [27] J.-M. Manceau, S. Zanotto, T. Ongarello, L. Sorba, A. Tredicucci, G. Biasiol, and R. Colombelli, “Mid-infrared intersubband polaritons in dispersive metal-insulator-metal resonators,” *Appl. Phys. Lett.* **105**, 081105 (2014).
- [28] J.-M. Manceau, G. Biasiol, N. L. Tran, I. Carusotto, and R. Colombelli, “Immunity of intersubband polaritons to inhomogeneous broadening,” *Phys. Rev. B* **96**, 235301 (2017).
- [29] P. G. Savvidis, J. J. Baumberg, R. M. Stevenson, M. S. Skolnick, D. M. Whittaker, and J. S. Roberts, “Angle-resonant stimulated polariton amplifier,” *Phys. Rev. Lett.* **84**, 1547–1550 (2000).
- [30] J. J. Baumberg, P. G. Savvidis, R. M. Stevenson, A. I. Tartakovskii, M. S. Skolnick, D. M. Whittaker, and J. S. Roberts, “Parametric oscillation in a vertical microcavity: A polariton condensate or micro-optical parametric oscillation,” *Phys. Rev. B* **62**, R16247 (2000).
- [31] J. Keeling, F. M. Marchetti, M. H. Szymańska, and P. B. Littlewood, “Collective coherence in planar semiconductor microcavities,” *Semicond. Sci. Technol.* **22**, R1 (2007).
- [32] H. P. Breuer and F. Petruccione, *The theory of open quantum systems* (Oxford University Press, 2002).
- [33] C. Cohen-Tannoudji, J. Dupont-Roc, and G. Grynberg, *Atom-photon interactions: basic processes and applications* (Wiley-VCH, Weinheim, 2004).
- [34] Q. Wu and X.-C. Zhang, “Free-space electro-optics sampling of mid-infrared pulses,” *Appl. Phys. Lett.* **71**, 1285 (1997).
- [35] R. Huber, A. Brodschelm, F. Tauser, and A. Leitenstorfer, “Generation and field-resolved detection of femtosecond electromagnetic pulses tunable up to 41 THz,” *Appl. Phys. Lett.* **76**, 3191 (2000).
- [36] K. Liu, J. Xu, and X.-C. Zhang, “GaSe crystals for broadband terahertz wave detection,” *Appl. Phys. Lett.* **85**, 863 (2004).
- [37] C. Kbler, R. Huber, S. Tbel, and A. Leitenstorfer, “Ultrabroadband detection of multi-terahertz field transients with GaSe electro-optic sensors: Approaching the near infrared,” *Appl. Phys. Lett.* **85**, 3360 (2004).
- [38] M. Porer, J.-M. Ménard, and R. Huber, “Shot noise reduced terahertz detection via spectrally postfiltered electro-optic sampling,” *Opt. Lett.* **39**, 2435 (2014).
- [39] S. Keiber, S. Sederberg, A. Schwarz, M. Trubetskoy, V. Pervak, F. Krausz, and N. Karpowicz, “Electro-optic sampling of near-infrared waveforms,” *Nature Photonics* **10**, 159 (2016).
- [40] M. Knorr, J. Raab, M. Tauer, P. Merkl, D. Peller, E. Wittmann, E. Riedle, C. Lange, and R. Huber, “Phase-locked multi-terahertz electric fields exceeding 13 MV/cm at a 190 kHz repetition rate,” *Opt. Lett.* **42**, 4367 (2017).
- [41] To obtain a better match with experimental data, we had to slightly modify the photon dispersion relation in the region of interest to
- $$\omega_C(k) = |k|/n + \omega_0, \quad (\text{A1})$$
- with a small  $\omega_0 = 20$  meV, so to include the consequences of, e.g., the leakage of electromagnetic radiation inside the metallic mirrors.
- [42] Another pump-only strategy to estimate polariton interactions is of course based on the electro-optical sampling of the time-dependence of the emission frequency during ring-down oscillation after a strong pulsed pump.
- [43] C. Ciuti and I. Carusotto, “Input-output theory of cavities in the ultrastrong coupling regime: The case of time-independent cavity parameters,” *Phys. Rev. A* **74**, 033811 (2006).